# Learning-Based Quantitative Microwave Imaging With a Hybrid Input Scheme

Lu Zhang, Kuiwen Xu, *Member, IEEE*, Rencheng Song, *Member, IEEE*, Xiuzhu Ye, *Senior Member, IEEE*, Gaofeng Wang, *Senior Member, IEEE*, and Xudong Chen, *Fellow, IEEE*

***Abstract*—In this letter, a learning-based inversion method with a hybrid input scheme is proposed to solve quantitative microwave imaging (MI) problems. The high-resolution dielectric targets are reconstructed by convolutional neural network (CNN) with a hybrid input scheme. The qualitative direct sampling method (DSM) is utilized to provide the spatial information, while the quantitative back propagation (BP) is employed to get the preliminary constitutive parameters of the unknown target. The hybrid input scheme, defined as an inner product of DSM and BP results (shorten as a DSM-BP scheme), significantly improves the reconstruction quality of U-net CNN compared to the BP-only input scheme without additional computational burden. The accuracy and stability of the proposed inversion are verified by both synthetic and experimental data.**

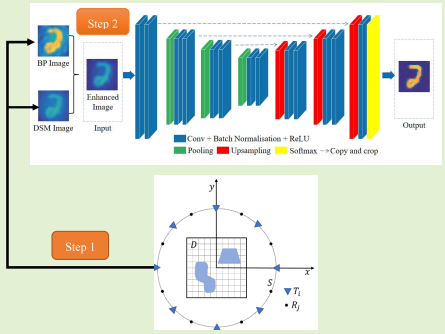


***Index Terms*— Back propagation (BP), convolutional neural network (CNN), direct sampling method (DSM), hybrid input scheme, quantitative microwave imaging (MI).**

## I. Introduction

MICORWAVE imaging (MI) is a promising noncontact and nondestructive imaging technology. In recent years, it has a wide range of applications in many fields, such as surveillance, microwave remote sensing, nondestruction detection, biomedical imaging and geological exploration [1]–[6]. Microwave imaging methods can be generally classified into two categories, i.e., qualitative methods and quantitative methods, according to whether constitutive parameters are reconstructed.

Qualitative imaging methods can only retrieve the shape, size and location of unknown scatterers within the domain of interest (DoI) [7]. Owing to the faster imaging speed compared to quantitative methods, qualitative inversion methods are preferred in some real-time imaging scenarios [8]–[13]. In comparison, quantitative imaging methods provide information about the constitutive properties (permittivity, conductivity) of the unknown scatterer [14]–[17] and are slower in imaging speed. Some hybrid methods are proposed to effectively solve quantitative MI [18], [19], which combine both the advantages of qualitative and quantitative methods. For example, linear sample method is used to provide the prior information in the nonlinear inversion [20]. Although these conventional hybrid methods can improve the accuracy of inversion and accelerate the convergence speed, they also require hundreds of iterations such that the computational cost is usually large, especially when dealing with the three-dimensional (3-D) quantitative MI. So, real-time quantitative microwave imaging methods are still urgently needed.

Due to strong nonlinear fitting ability and one-step calculation after the training procedure, deep learning methods have been adopted in the electromagnetics and pave the way to real-time quantitative MI [21]–[24]. For example, in [22], [23], the preliminary results got by some

Manuscript received June 13, 2020; revised July 23, 2020; accepted July 23, 2020. Date of publication July 27, 2020; date of current version November 18, 2020. This work was supported in part by the Zhejiang Provincial Natural Science Foundation of China under Grant LY19F010012; in part by the National Natural Science Foundation of China under Grant 61971174; in part by the Talent Project of Zhejiang Association for Science and Technology under Grant SKX201901; and in part by the China Postdoctoral Science Foundation under Grant 2019M661984. The associate editor coordinating the review of this article and approving it for publication was Dr. Marko Vauhkonen. *(Corresponding author: Kuiwen Xu.)*

Lu Zhang, Kuiwen Xu, and Gaofeng Wang are with the Engineering Research Center of Smart Microsensors and Microsystems, Ministry of Education, Hangzhou Dianzi University, Hangzhou 310018, China (e-mail: kuiwenxu@hdu.edu.cn).

Rencheng Song is with the Department of Biomedical Engineering, Hefei University of Technology, Hefei 230009, China (e-mail: rcsong@hfut.edu.cn).

Xiuzhu Ye is with the School of Information and Electronics Engineering, Beijing Institute of Technology, Beijing 100811, China (e-mail:xiuzhuye@outlook.com)

Xudong Chen is with the Department of Electrical and Computer Engineering, National University of Singapore, Singapore 117583 (e-mail: elechenx@nus.edu.sg).

Digital Object Identifier 10.1109/JSEN.2020.3012177

noniterative quantitative inversion schemes, e.g., the back propagation (BP), are employed to feed the convolutional neural network (CNN) in learning-based methods and they can achieve good results in almost real-time. And in [24], instead of directly using deep neural networks (DNNs) for nonlinear inversion, they are used for the solution of the time-consuming gradient in the traditional objective function approach. All of these works have demonstrated the effectiveness of learning-based methods for the quantitative MI in terms of accuracy and efficiency.

In this letter, in virtue of qualitative method, e.g., DSM, a learning-based inversion method with a hybrid input scheme in frame of CNN is proposed to solve the quantitative MI problems in real-time. The DSM only involves a simple inner product calculation and has good stability under high-level noise, which can be used to get the qualitative information regarding the shape and location of the scatterers. The enhanced images can be obtained by the inner product of the preliminary constitutive parameters through BP and the retrieval spatial distribution by DSM. Taking the obtained profiles as inputs of the CNN, more accurate images with high frequency components can be finally got by the CNN. More available knowledge on underlying physic is obtained by the DSM before entering into the CNN. The novelty of this letter is summarized as follows: 1) The enhanced synthetic images by the inner product of the reconstructed profiles by DSM and BP, are incorporated as the hybrid inputs of U-net CNN [22], [25]. Compared to CNN cooperating with only BP, the proposed method can greatly improve the imaging accuracy, and almost no extra computation cost is added. 2) Not restricted to DSM and BP, the presented hybrid method provides a general and effective framework for achieving fast and approximate quantitative MI.

## II. Formulation of the Problem

As illustrated in Fig. 1, a two-dimensional (2-D) inverse scattering problems (ISPs) with the transverse magnetic (TM) polarized wave is considered and time harmonic fields are assumed with $\exp(-i\omega t)$ notation. In a homogeneous medium background with the permittivity $\epsilon_0$ and permeability $\mu_0$ (free space herein), the unknown scatterers are located in the domain of interest (DoI) $D$ ($D \subset R^2$). There are totally $N_i$ transmitters around the DoI located at $T_i$ in the measurement domain $S$. For each incidence, the scattered fields are collected by the $N_r$ receivers located at $R_j$ ($j$=1, 2, …, $N_r$), in the measurement domain $S$. The goal of the quantitative MI is to reconstruct the information (such as the shape, position, and constitutive parameters) of the unknown scatterers from a multistatic response (MSR) matrix with the size of $N_i \times N_r$.

For the $l$th incidence, the total electric field satisfies the following source-type integral equations in the DoI:

$$E_l^{\text{tot}}(\mathbf{r}) = E_l^{\text{inc}}(\mathbf{r}) + k_0^2 \int_D G(\mathbf{r}, \mathbf{r}') I_l(\mathbf{r}') d\mathbf{r}' \quad for\ \mathbf{r} \in D, \quad (1)$$

where $E_l^{\text{inc}}(\mathbf{r})$ denotes the incident electric field located at $\mathbf{r}$, $G(\mathbf{r}, \mathbf{r}')$ is the 2-D Green's function for the homogenous medium and $k_0 = \omega\sqrt{\epsilon_0\mu_0}$ is the wavenumber of the homogenous background. The induced current $J_l(\mathbf{r})$ can be

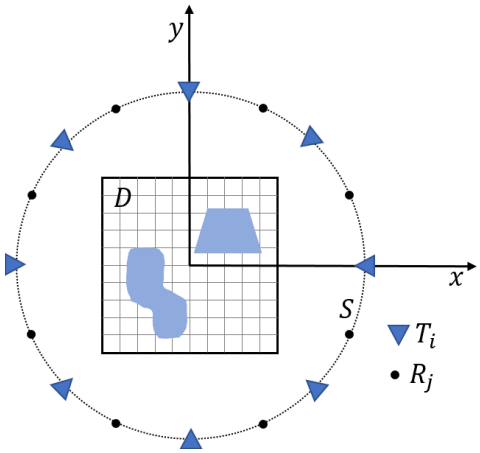


Fig. 1. The geometric model of the quantitative MI.

expressed as,

$$J_l(\mathbf{r}) = -i\omega\epsilon_0(\epsilon(\mathbf{r})/\epsilon_0 + i\sigma(\mathbf{r})/\omega\epsilon_0 - 1)E_l^{\text{tot}}(\mathbf{r}) \quad for\ \mathbf{r} \in D, \quad (2)$$

where $\epsilon(\mathbf{r})$ and $\sigma(\mathbf{r})$ denote the permittivity and conductivity of the unknown scatterers in the DoI, respectively. Herein, the dielectric scatterers ($\sigma = 0$) are considered for inversion. For convenience, we defined the contrast source in (1) as $I_l(\mathbf{r}) = \frac{J_l(\mathbf{r})}{-i\omega\epsilon_0} = (\epsilon(\mathbf{r})/\epsilon_0 - 1)E_l^{\text{tot}}(\mathbf{r})$ and $\epsilon(\mathbf{r})/\epsilon_0 - 1$ is denoted as the unknown contrast function $\chi(\mathbf{r})$ [7].

The scattered field at measurement domain $S$ can be formulated as,

$$E_l^{\text{sca}}(\mathbf{r}) = k_0^2 \int_D G(\mathbf{r}, \mathbf{r}') I_l(\mathbf{r}') d\mathbf{r}' \quad for\ \mathbf{r} \in S. \quad (3)$$

Equations (1) and (3) depict the forward problem and are denoted as the state equation and the data equation, respectively [7]. In the numerical calculation, the DoI $D$ is discretized into $M = M_1 \times M_2$ small subunits (the numbers of subunits along the $x-$ and $y-$axes are $M_1$ and $M_2$, respectively). Thus, the discretized form of (1) and (3) can be expressed as,

$$\bar{E}_l^{\text{tot}} = \bar{E}_l^{\text{inc}} + \bar{\bar{G}}_D \cdot \bar{I}_l, \quad (4)$$

$$\bar{E}_l^{\text{sca}} = \bar{\bar{G}}_S \cdot \bar{I}_l, \quad (5)$$

where $\bar{\bar{G}}_D$ represents the Green's function mapping from the induced current to the scattered field in the DoI $D$, and $\bar{\bar{G}}_S$ is the Green's function operator mapping the induced current to the scattered field at the domain of measurements $S$ [7].

For inverse problem, the task is to reconstruct the unknown contrast function $\chi(\mathbf{r})$, $\mathbf{r} \in D$ from the measured scattered fields $\bar{E}_{l,\text{mea}}^{\text{sca}}(\mathbf{r})$, $\mathbf{r} \in S$. And the inverse problem is usually casted into the model-based optimization problem, which can be expressed as,

$$\text{Min}: \ f(\bar{\chi}) = \sum_{l=1}^{N_i} \|F(\bar{\chi}, \bar{E}_l^{\text{inc}}) - \bar{E}_{l,\text{mea}}^{\text{sca}}\|_S^2 + \alpha R(\bar{\chi}), \quad (6)$$

where $F$ denotes the operator of the forward solver, i.e., $\bar{E}_l^{\text{sca}} = F(\bar{\chi}, \bar{E}_l^{\text{inc}})$ and $\|\cdot\|_S$ denotes the Euclidian length of a vector on the domain of $S$, $R(\bar{\chi})$ is a nonnegative

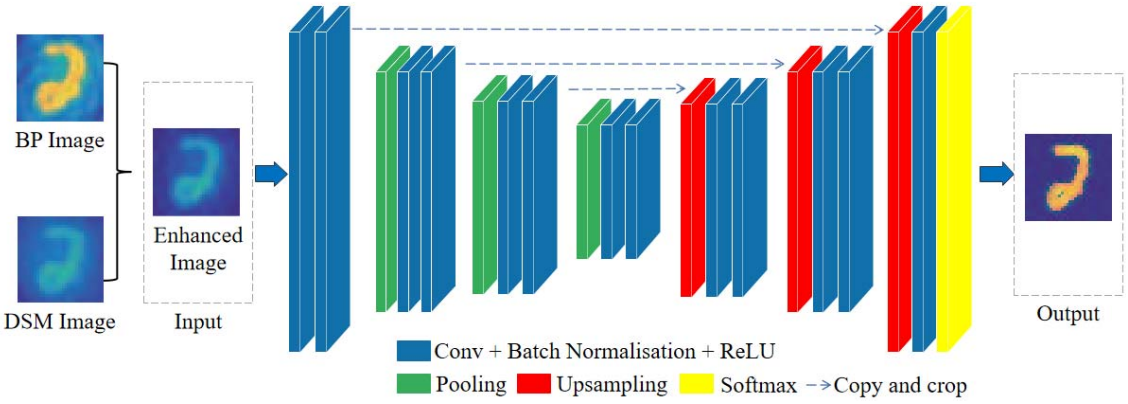


Fig. 2. U-net architecture for the quantitative MI.

regularizing term, which is used to obtain a stable solution, and the $\alpha$ is the weighting parameter. In order to alleviate the nonlinearity and ill-posedness of quantitative MI based ISPs, many nonlinear iterative inversion methods have been proposed [14]–[17]. However, they usually consume large amount of computational resources. Therefore, a learning-based inversion method in the frame of CNN with a hybrid input scheme based on the DSM coupled with BP is proposed to realize real-time quantitative MI.

## III. Inversion of Deep Learning-Based Methods

In this paper, the classic U-net CNN mentioned is employed to solve the quantitative MI [25]. As illustrated in Fig. 2, there are four layers in the U-net CNN, and it consists of a contracting path and an expansive path, which exhibits an U-shaped architecture [25]. The contracting path (left side) is a typical convolutional network that consists of repeated application of two $3\times3$ convolutions, each followed by a batch normalization (BN) [26], a rectified linear unit (ReLU) and an $2 \times 2$ max pooling operation. In the training of the neural networks, batch normalization in the U-net CNN is used for accelerating the training of deep network by reducing internal covariance shift. It not only makes the network more stable but also guarantees the nonlinear expression ability of the model [26]. In this paper, the results got by BP and BP-DSM are directly taken as the inputs of the CNNs. Herein, no other normalization operation on the input feature maps is used.

During the process of contraction, the spatial information decreases while feature information increases. The expansive path (right side) combines the feature and spatial information through a sequence of $3 \times 3$ up-convolutions and concatenations with high-resolution features from the contracting path. Using the preliminary results obtained by noniterative inversion method as the inputs of U-net, this ensures the one-to-one corresponding relationship between the input and the output in the training and the trained U-net network can realize real-time quantitative MI.

### A. BP Scheme

Back propagation (BP) is a fast noniterative inversion method widely used in the microwave and optical imaging communities, which can supply quantitative information. The basic procedure for the formulation of BP is introduced in [7], which basically consists of three steps. Firstly, the contrast source is assumed to be proportional to the back-propagated field in the BP scheme, i.e., $\bar{I} = \gamma \cdot \bar{\bar{G}}_S^H \cdot \bar{E}^{\mathrm{sca}}$, where the superscript $H$ denotes the conjugate transpose operation. The complex constant $\gamma$ can be got by the minimization of (6) as follows,

$$\gamma = \frac{\langle \bar{E}^{\mathrm{sca}}, \bar{\bar{G}}_S \cdot (\bar{\bar{G}}_S^H \cdot \bar{E}^{\mathrm{sca}}) \rangle_S}{\| \bar{\bar{G}}_S \cdot (\bar{\bar{G}}_S^H \cdot \bar{E}^{\mathrm{sca}}) \|_S}, \tag{7}$$

where $\langle A, B \rangle_S$ denotes the inner product of vectors $A$ and $B$ in the domain $S$. Then, calculate the total field in the DoI by (4). Finally, for the $l$th incidence, the definition of $\chi(\mathbf{r})$ requires $\bar{I}_l = \bar{\bar{\chi}} \cdot \bar{E}_l^{\mathrm{tot}}$. And all incidences lead to a least squares problem, and the contrast function can be obtained as follows,

$$\chi(\mathbf{r}) = \frac{\sum_{l=1}^{N_i} \bar{I}_l(\mathbf{r}) \cdot [\bar{E}_l^{\mathrm{tot}}(\mathbf{r})]^*}{\sum_{l=1}^{N_i} \| \bar{E}_l^{\mathrm{tot}}(\mathbf{r}) \|^2}, \tag{8}$$

where the superscript $*$ denotes the complex conjugate operation. Through the BP, the transformation from the measured scattered fields to the preliminary quantitative image can be achieved. The results obtained by BP are often used as initial guesses, which can accelerate the convergence speed of iterative inversion methods, and also can effectively reduce the probability of falling into the local minima. Since the BP can quickly obtain approximate information of unknown scatterers, it is often used as an input scheme in learning-based inversion methods [22], [23].

### B. BP-DSM Scheme

To fulfill the one-to-one relationship with the neural network, a hybrid input scheme, i.e., the dot product between the result by DSM and the one by BP (denoted as BP-DSM scheme), is proposed to achieve the quantitative inversion. The results obtained by BP are used for distinguishing scatterers with the same shape but different permittivity, and the spatial information obtained by DSM can also improve the quality of feature map information compared to the one by only BP.

In qualitative methods, an appropriate indicator function is defined on the DoI, which determines whether a sampling point $r_p$ ($p = 1, 2, \ldots, M$) lies inside or outside the unknown scatterers. The indicator function in multiple incidences can be expressed as [12], [13],

$$\Psi(r_p) = \frac{1}{N_i} \sum_{l=1}^{N_i} \frac{| \langle \bar{E}_l^{\text{sca}}(\mathbf{r}), \bar{G}_S(\mathbf{r}, r_p) \rangle_S |}{\| \bar{E}_l^{\text{sca}}(\mathbf{r}) \|_S \| \bar{G}_S(\mathbf{r}, r_p) \|_S}. \tag{9}$$

For the single sampling point $r_p$, the dimensions of the vector $\bar{E}_l^{\text{sca}}(\mathbf{r})$ and vector $\bar{G}_S(\mathbf{r}, r_p)$ both are $N_r \times 1$, where $\mathbf{r}$ indicates the location vector of receivers, and $N_r$ denotes the number of the receivers. Then the indicator function can determine whether the sampling point $r_p$ lies inside the scatterer when the following two conditions are satisfied: (i) the DoI is finely meshed, (ii) the sampling point $r_p$ is far from the measurement domain $S$. Specifically, if $\Psi(r_p) \approx 1$, the sampling point $r_p$ is within the unknown scatterers, and if $\Psi(r_p) \approx 0$, the sampling point $r_p$ belongs to background medium. An alterative way is to set a threshold value $\zeta$ for $\Psi(r_p)$. The sampling point $r_p$ is out of the support of the scatterer if $\Psi(r_p)$ is less than $\zeta$, and $\Psi(r_p)$ is set to zero. Otherwise, it is within the scatterer and $\Psi(r_p)$ remains unchanged. Since the indicator function $\Psi(r_p)$ only involves the inner product between the Green's function and the scattered field, it is easy to implement and has a small amount of calculation.

Therefore, DSM can well transform the scattered field into the distribution profile of scatterer. However, DSM can only qualitatively judge whether the sampling point is inside the scatterer, but cannot provide quantitative information. For example, when dealing with the scatterers with the same shape but different constitutive parameters (i.e., permittivity and conductivity), the distribution profiles of the indicator function of the scatterers could not be clearly distinguished. If the results by DSM are directly used as the inputs of CNN, the output profiles by CNN can not be effectively reconstructed. In this case, the input-output mapping relationship with the CNN would not be an injection function and therefore could not be well trained. Consequently, a hybrid input scheme with both of BP and DSP is utilized to achieve fast quantitative MI.

## IV. Numerical Results

In this section, some numerical tests are used to test the performance of the hybrid BP-DSM scheme based on U-net CNN. In order to quantitatively compare the reconstruction quality, the reconstruction error for a single profile is defined as

$$\text{ERR}^{\text{tot}} = \sqrt{\frac{1}{M} \sum_m \sum_n \left| \frac{\bar{\bar{\epsilon}}_{r;m,n}^{\text{r}} - \bar{\bar{\epsilon}}_{r;m,n}^{\text{t}}}{\bar{\bar{\epsilon}}_{r;m,n}^{\text{t}}} \right|^2}, \tag{10}$$

where $\bar{\bar{\epsilon}}_{r;m,n}^{r}$ and $\bar{\bar{\epsilon}}_{r;m,n}^{t}$ ($m = 1, 2, \ldots, M_1, n = 1, 2, \ldots, M_2$) are the reconstructed and true relative permittivity of the unknown scatterers, respectively, and $M = M_1 \times M_2$ is the total number of small subunits. To further evaluate the reconstruction qualities exactly on the unknown scatterers, another type of relative reconstructed error $\text{ERR}^{\text{sct}}$ is defined with the summation of indexes over only the domain where unknown scatterers distribute.

To evaluate the overall merits of the proposed method, the average of reconstructed errors on all test samples within the testing set calculated as

$$R_e = \frac{1}{M_t} \sum_{i=1}^{M_t} \text{ERR}^{\text{tot}}(i), \tag{11}$$

where the $M_t$ denotes the total number of samples within the testing set.

### A. Tests With Synthetic Data

The MNIST dataset is used to train the CNN and it is a database containing 10 handwritten digits (from 0 to 9). Here, a domain of interest (DoI) $D$ of $2 \times 2$ m$^2$ is considered, which is discretized into $32 \times 32$ pixels. The operating frequency is 400 MHz and there are 20 line sources and 40 line receivers evenly placed on a circle denoted by $S$ with a radius of 3 m centered at the origin. The digit-like objects are set to be lossless dielectrics with the relative permittivity of 1.5 as shown in Fig. 3(a). By a full-wave electromagnetic scattering solver, the multistatic response (MSR) matrix generated by an array of transceivers with the size of $N_r \times N_i$ can be obtained. The quantitative inversion is to reconstruct the values of the $M$ complex relative permittivities from this MSR matrix.

In the training stage, we randomly select 5,000 images from the MNIST dataset and set their relative permittivities randomly within the range of [1.1, 1.5]. It is noted that the CNN is trained with the noiseless scattered field data. Meanwhile, 4,000 images are randomly selected as the training dataset, and 1,000 images are used for testing the established CNN. And different training schemes are used to transform the scattered fields into the rough images in the training stage. The true profiles in the training are considered as the exact outputs in CNN. In the testing, 10% additional white Gaussian noise (AWGN) is added to the MSR matrix.

In the first example, the 1,000 images from the MNIST dataset are used for testing. In the testing stage, a group composed of 16 profiles is used for comparison as depicted in Fig. 3(a). Fig. 3(b) and (c-1) show the retrieval results obtained by DSM and BP, respectively. It is worthy mentioning that the time taken by DSM to convert scattered fields into a qualitative image is about 0.4s, which is almost negligible compared with the time spent by BP (about 3s). For the results obtained from DSM, we can set a threshold ratio, i.e., $\delta$ to distinguish whether the sampling point (i.e., $r_p$) belongs to the scaterers or not. If $\Psi(r_p)$ is smaller than a threshold value ($\zeta = \delta \times \max(\Psi)$), the sample point is deemed to be out of the scatterers. Fig. 3(c-2), (c-3), and (c-4) show the hybrid BP-DSM results with different threshold ratios, i.e., 0, 0.1 and 0.2, respectively. One can see that after incorporating the spatial information got by DSM into the results by BP, the improved profiles can be obtained especially for the background. Owing to the quantitative information supplied by BP, the BP-DSM can be utilized for quantitative MI. Fig. 3(d-1) shows the final reconstruction results predicted by the CNN under the BP scheme. Fig. 3(d-2), (d-3), and (d-4) depict the final reconstruction results predicted by the CNN under the BP-DSM scheme with $\delta = 0$, 0.1, and 0.2,

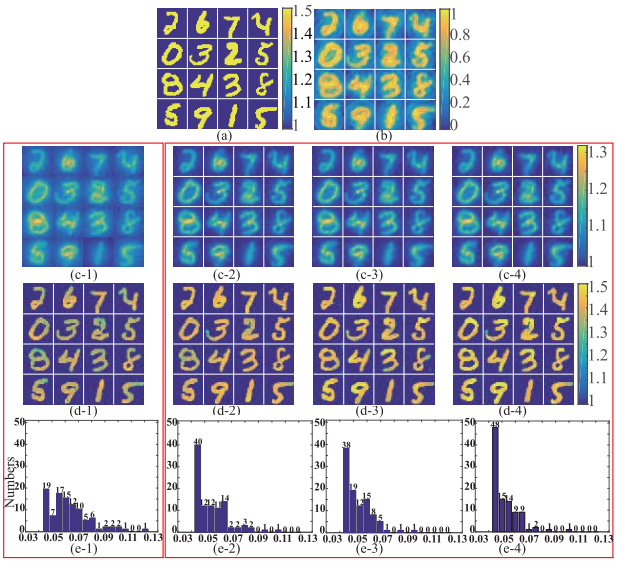


Fig. 3. Reconstruction results of digit-like objects with $\epsilon_r = 1.5$. (a) Sixteen ground truths; Reconstruction results by (b) the DSM and (c-1) the BP, respectively; (c-2) to (c-4) show the hybrid BP-DSM results with the different threshold ratios $\delta = 0$, 0.1, and 0.2, respectively; Reconstruction results by U-net CNN under (d-1) the BP scheme and (d-2, d-3, d-4) the BP-DSM scheme with $\delta = 0$, 0.1, and 0.2, respectively. (e-1) to (e-4) show the reconstruction error $\mathrm{ERR}^{\mathrm{tot}}$ distribution of 100 profiles by BP and hybrid BP-DSM scheme with $\delta = 0$, 0.1, and 0.2, respectively.

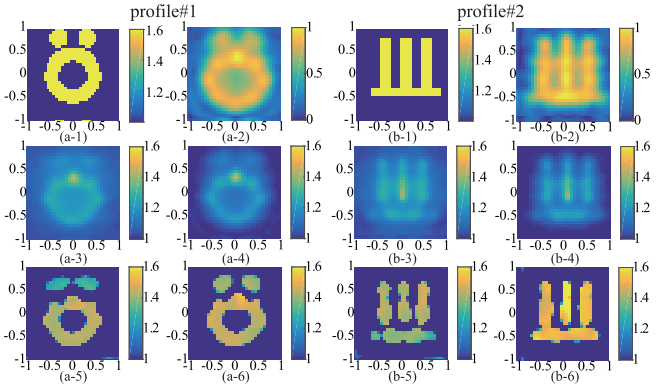


Fig. 4. (a-1) and (b-1) show the exact profiles; (a-2) to (a-6) show the results for the "profile#1" by DSM, BP, hybrid BP-DSM, the U-net CNN under BP scheme and BP-DSM scheme, respectively; (b-2) to (b-6) show the results for the "profile#2" by DSM, BP, hybrid BP-DSM, the U-net CNN under BP scheme and BP-DSM scheme, respectively.

TABLE I
THE RECONSTRUCTION ERRORS OF TWO PROFILES

| | profile#1 | | profile#2 | |
|---|---|---|---|---|
| | $\mathrm{ERR}^{\mathrm{tot}}$ | $\mathrm{ERR}^{\mathrm{sct}}$ | $\mathrm{ERR}^{\mathrm{tot}}$ | $\mathrm{ERR}^{\mathrm{sct}}$ |
| BP scheme | 0.1278 | 0.1146 | 0.1273 | 0.1089 |
| BP-DSM scheme | 0.1070 | 0.0928 | 0.0941 | 0.0743 |

respectively. It is validated that the BP-DSM scheme has better reconstruction performance than the BP scheme. In the testing stage, with the trained U-net CNN, the average time for testing a sample is about 0.596s, which is almost negligible compared to the one used by traditional iterative inversion methods. In order to quantitatively compare the two schemes, Fig. 3(e-1), (e-2), (e-3), and (e-4) show the relative errors $\mathrm{ERR}^{\mathrm{tot}}$ distribution of the reconstructed 100 profiles randomly selected from testing set. The average errors $R_e$ of BP scheme and hybrid BP-DSM scheme, when the threshold ratio $\delta$ being 0, 0.1, and 0.2, are 0.0616, 0.0524, 0.0520, and 0.0501, respectively. One can see from the bar chart that, the errors distribution of the results obtained by the BP-DSM scheme is more concentrated on the parts of small errors, and the reconstructed results are more accurate. The case of $\delta$ being equal to 0.3 is also tested and the average retrieval error, i.e., $R_e$, is 0.0509, and it shows no improvement when the ratio $\delta$ being greater than 0.2. Consequently, it is proven that the proposed hybrid input scheme can effectively improve the quality of reconstruction results.

In order to investigate the generalization ability of the proposed learning-based method (here, $\delta = 0.2$ is chosen as default), two profiles with the relative permittivity of 1.6, totally different from the MNIST database, are used for numerical experiments as illustrated in Fig. 4(a-1) and (b-1). In this example, all the configurations and settings in the training are the same as the example 1. Fig. 4 shows the retrieval results by the proposed learning-based inversion method with two different schemes. Fig. 4(a-2) to (a-6) show the results for the case of "profile#1" by DSM, BP, hybrid BP-DSM, the U-net CNN under the BP scheme and the BP-DSM scheme, respectively. And Fig. 4(b-2) to (b-6) show the results for the "profile#2" by DSM, BP, hybrid BP-DSM, the U-net CNN under BP scheme and BP-DSM scheme, respectively. As can be seen from these results, that the reconstruction results by the BP, i.e., the shapes and the permittivities, are not accurate, whereas the retrieval shapes of the unknown scatterers got by DSM are better. With the inner product between the DSM and the BP, the enhanced results can be obtained. Hybrid BP-DSM results show DSM can improve the results of BP and make the background more clear. The results by BP and hybrid BP-DSM are used as the inputs of the CNN for comparison. It can be seen clearly that the results by BP-DSM scheme are significantly improved. Table I shows the reconstruction errors of these two results. It can be observed that the retrieval results obtained by the BP-DSM scheme have smaller reconstructed errors. It is further validated that the spatial information obtained by the hybrid input scheme can effectively improve the imaging quality.

### B. Tests With Experimental Data

In the last example, the "*FoamDielExt*" experimental data from 2 to 10 GHz provided by the Institute Fresnel [27], is used for the test. And detailed information on the configuration of the experimental measurement setup can be found in [27]. In the DoI of 20 cm $\times$ 20 cm, the "*FoamDielExt*" profile is depicted in Fig. 5(a), which consists of two scatterers, where a smaller cylinder with the relative permittivity of 3.0, the diameter of 3.1 cm, and a large cylinder with relative permittivity of 1.45, the diameter of 8 cm. Due to the lossless scatterers, the null imaginary part of the profile is not shown. In the inversion, a 32 $\times$ 32 grid mesh of the DoI is used. In experimental test, we use a new training data set

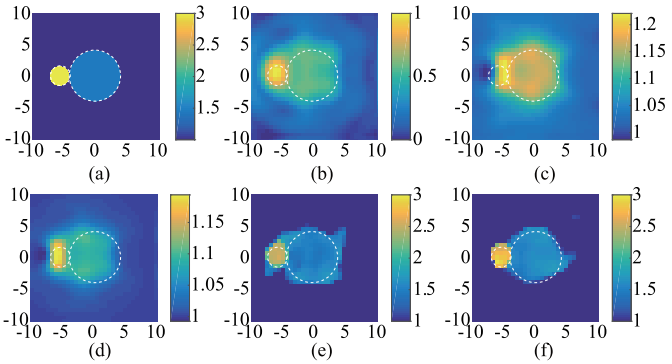


Fig. 5. (a) "*FoamDielExt*" profile (ground truth). (b)-(f) The reconstruction results by DSM, BP, hybrid BP-DSM, U-net CNN under BP scheme, and the one under the hybrid BP-DSM scheme, respectively.

slightly different from the numerical tests above to train the U-net CNN.

In the training, in order to improve the diversity of the samples, a cylinder with random position, size, and its relative permittivity randomly distributed in the range of [1.5, 3.3] are embedded in each "MNIST" profile. And the noiseless synthetic data is used to train the CNN, then the network can be tested by the measured data. The reconstruction results at 4 GHz by DSM, BP, hybrid BP-DSM, the U-net CNN under BP scheme and BP-DSM scheme are shown in Fig. 5(b), (c), (d), (e), and (f), respectively. The reconstruction errors $\mathrm{ERR}^{\mathrm{tot}}$ by BP and BP-DSM schemes, are 0.1858, and 0.1631, respectively. It can be seen that the learning-based method with the hybrid input scheme can obtain better imaging performance.

## V. Conclusion

Although the qualitative methods cannot reconstruct the constitutive parameters of the unknown targets, they can effectively reduce the probability of falling into a false solution and accelerate the convergence speed through using the obtained spatial information as the prior information in the quantitative inversion. Inspired by this, a learning-based inversion method by convolutional neural network (CNN) with the hybrid input scheme, i.e, DSM coupled with BP, is proposed to solve quantitative MI problems. The input feature map can be greatly enhanced by the inner product of the physical retrieval electrical parameters through BP and the spatial retrieval distribution with DSM. Taking the hybrid scheme as inputs of the network, the CNN can easily learn the underlying relationship between the input feature maps and the output profiles. Numerical examples show that the results obtained by CNN under BP-DSM scheme are superior to the one under BP scheme. Although DSM can not directly reconstruct the constitutive parameters of the unknown targets, the learning-based method with the hybrid input scheme can achieve the quantitative MI in real-time and effectively improve the reconstruction performance in terms of accuracy and efficiency.

## References

[1] R. Chandra, H. Zhou, I. Balasingham, and R. M. Narayanan, "On the opportunities and challenges in microwave medical sensing and imaging," *IEEE Trans. Biomed. Eng.*, vol. 62, no. 7, pp. 1667–1682, Jul. 2015.

[2] S. Caorsi, A. Massa, M. Pastorino, and M. Donelli, "Improved microwave imaging procedure for nondestructive evaluations of two-dimensional structures," *IEEE Trans. Antennas Propag.*, vol. 52, no. 6, pp. 1386–1397, Jun. 2004.

[3] M. S. Zhdanov, *Geophysical Inverse Theory and Regularization Problems*. Amsterdam, The Netherlands: Elsevier, 2002.

[4] K. D. Paulsen, S. P. Poplack, D. Li, M. W. Fanning, and P. M. Meaney, "A clinical prototype for active microwave imaging of the breast," *IEEE Trans. Microw. Theory Techn.*, vol. 48, no. 11, pp. 1841–1853, Nov. 2000.

[5] M. A. Aldhaeebi, T. S. Almoneef, H. Attia, and O. M. Ramahi, "Near-field microwave loop array sensor for breast tumor detection," *IEEE Sensors J.*, vol. 19, no. 24, pp. 11867–11872, Dec. 2019.

[6] B. Wang, Y. Sun, Z. Wang, and X. Wang, "Three-dimensional microwave-induced thermoacoustic imaging based on compressive sensing using an analytically constructed dictionary," *IEEE Trans. Microw. Theory Techn.*, vol. 68, no. 1, pp. 377–386, Jan. 2020.

[7] X. Chen, *Computational Methods for Electromagnetic Inverse Scattering*. Hoboken, NJ, USA: Wiley, 2018.

[8] G. G. Bellizzi, M. T. Bevacqua, L. Crocco, and T. Isernia, "3-D field intensity shaping via optimized multi-target time reversal," *IEEE Trans. Antennas Propag.*, vol. 66, no. 8, pp. 4380–4385, Aug. 2018.

[9] X. Chen and K. Agarwal, "MUSIC algorithm for two-dimensional inverse problems with special characteristics of cylinders," *IEEE Trans. Antennas Propag.*, vol. 56, no. 6, pp. 1808–1812, Jun. 2008.

[10] D. Colton and A. Kirsch, "A simple method for solving inverse scattering problems in the resonance region," *Inverse Problems*, vol. 12, no. 4, p. 383, 1996.

[11] I. Catapano, L. Crocco, and T. Isernia, "On simple methods for shape reconstruction of unknown scatterers," *IEEE Trans. Antennas Propag.*, vol. 55, no. 5, pp. 1431–1436, May 2007.

[12] K. Ito, B. Jin, and J. Zou, "A direct sampling method to an inverse medium scattering problem," *Inverse Problems*, vol. 28, no. 2, Feb. 2012, Art. no. 025003.

[13] S. Kang, M. Lambert, and W.-K. Park, "Analysis and improvement of direct sampling method in the monostatic configuration," *IEEE Geosci. Remote Sens. Lett.*, vol. 16, no. 11, pp. 1721–1725, Nov. 2019.

[14] W. C. Chew and Y. M. Wang, "Reconstruction of two-dimensional permittivity distribution using the distorted born iterative method," *IEEE Trans. Med. Imag.*, vol. 9, no. 2, pp. 218–225, Jun. 1990.

[15] M. Li, O. Semerci, and A. Abubakar, "A contrast source inversion method in the wavelet domain," *Inverse Problems*, vol. 29, no. 2, Feb. 2013, Art. no. 025015.

[16] X. Ye, X. Chen, Y. Zhong, and K. Agarwal, "Subspace-based optimization method for reconstructing perfectly electric conductors," *Prog. Electromagn. Res.*, vol. 100, pp. 119–128, Jan. 2010.

[17] Y. Zhong and X. Chen, "An FFT twofold subspace-based optimization method for solving electromagnetic inverse scattering problems," *IEEE Trans. Antennas Propag.*, vol. 59, no. 3, pp. 914–927, Mar. 2011.

[18] I. Catapano, L. Crocco, M. D'Urso, and T. Isernia, "On the effect of support estimation and of a new model in 2-D inverse scattering problems," *IEEE Trans. Antennas Propag.*, vol. 55, no. 6, pp. 1895–1899, Jun. 2007.

[19] L. Crocco, I. Catapano, L. Di Donato, and T. Isernia, "The linear sampling method as a way to quantitative inverse scattering," *IEEE Trans. Antennas Propag.*, vol. 60, no. 4, pp. 1844–1853, Apr. 2012.

[20] K. Agarwal, X. Chen, and Y. Zhong, "A multipole-expansion based linear sampling method for solving inverse scattering problems," *Opt. Express*, vol. 18, no. 6, pp. 6366–6381, 2010.

[21] A. Massa, D. Marcantonio, X. Chen, M. Li, and M. Salucci, "DNNs as applied to electromagnetics, antennas, and propagation—A review," *IEEE Antennas Wireless Propag. Lett.*, vol. 18, no. 11, pp. 2225–2229, Nov. 2019.

[22] Z. Wei and X. Chen, "Deep-learning schemes for full-wave nonlinear inverse scattering problems," *IEEE Trans. Geosci. Remote Sens.*, vol. 57, no. 4, pp. 1849–1860, Apr. 2019.

[23] L. Li, L. G. Wang, F. L. Teixeira, C. Liu, A. Nehorai, and T. J. Cui, "DeepNIS: Deep neural network for nonlinear electromagnetic inverse scattering," *IEEE Trans. Antennas Propag.*, vol. 67, no. 3, pp. 1819–1825, Mar. 2019.

[24] R. Guo, X. Song, M. Li, F. Yang, S. Xu, and A. Abubakar, "Supervised descent learning technique for 2-D microwave imaging," *IEEE Trans. Antennas Propag.*, vol. 67, no. 5, pp. 3550–3554, May 2019.

[25] O. Ronneberger, P. Fischer, and T. Brox, "U-Net: Convolutional networks for biomedical image segmentation," in *Proc. 18th Int. Conf. Med. Image Comput. Comput.-Assist. Intervent. (MICCAI)*, pp. 234–241, 2015.

[26] S. Ioffe and C. Szegedy, "Batch normalization: Accelerating deep network training by reducing internal covariate shift," 2015, *arXiv:1502.03167*. [Online]. Available: http://arxiv.org/abs/1502.03167
[27] J.-M. Geffrin, P. Sabouroux, and C. Eyraud, "Free space experimental scattering database continuation: Experimental set-up and measurement precision," *Inverse Problems*, vol. 21, no. 6, pp. 117–130, 2005.

**Lu Zhang** received the B.E. degree from Nanchang Hangkong University, Nanchang, China, in 2018. She is currently pursuing the M.S. degree with Hangzhou Dianzi University. Her current research interests include microwave imaging and electromagnetic inverse scattering problems.

**Kuiwen Xu** (Member, IEEE) received the B.E. degree from Hangzhou Dianzi University, Hangzhou, China, in 2009, and the Ph.D. degree from Zhejiang University, Hangzhou, China, in 2014, both in electrical engineering. From 2012 to 2013, he was a Visiting Ph.D. Student with the National University of Singapore, Singapore. From 2014 to 2015, he was a Senior Researcher with Huawei Technologies Company Ltd., Hangzhou. He was invited to the State Key Laboratory of Terahertz and Millimeter Waves, City University of Hong Kong, Hong Kong, in 2018, as a Visiting Professor. Since September 2015, he has been with Hangzhou Dianzi University, Hangzhou, where he is currently an Associate Professor. His research interests include electromagnetic inverse problems, microwave measurement, and novel antenna design.

**Rencheng Song** (Member, IEEE) received the B.S. degrees in mathematics from Jilin University, Changchun, China, in 2005, and the Ph.D. degree from Zhejiang University, Hangzhou, China, in 2010. He is currently an Associate Professor with the Department of Biomedical Engineering, Hefei University of Technology. His research interests include intelligent perceptions for biomedical measurements, such as video-based physiological parameter measurement, electromagnetic imaging, and machine learning.

**Xiuzhu Ye** (Senior Member, IEEE) received the B.E. degree in telecommunication engineering from the Harbin Institute of Technology, Harbin, China, in 2008, and the Ph.D. degree from the Department of Electrical and Computer Engineering, National University of Singapore, Singapore, in 2012. From 2012 to 2013, she worked at the Department of Electrical and Computer Engineering, National University of Singapore, as a Research Fellow. Since 2013, she worked as an Assistant Professor with Beihang University. Since 2019, she has been an Associate Professor with the School of Information and Electronics, Beijing Institute of Technology. Her research interests include electromagnetic inverse problems, microwave imaging methods, and antenna designing. She has served on review boards of various technical journals, including the IEEE TRANSACTIONS ON ANTENNAS AND PROPAGATION, the IEEE TRANSACTIONS ON MICROWAVE THEORY AND TECHNIQUES, *Radio Science*, and *Optics Express*.

**Gaofeng Wang** (Senior Member, IEEE) received the Ph.D. degree in electrical engineering from the University of Wisconsin-Milwaukee, Milwaukee, WI, USA, in 1993, and the Ph.D. degree in scientific computing from Stanford University, Stanford, CA, USA, in 2001. He was a Scientist with Tanner Research Inc., Pasadena, CA, from 1993 to 1996. He was a Principal Researcher and a Development Engineer with Synopsys Inc., Mountain View, CA, from 1996 to 2001. In 1999, he served as a Consultant with Bell Laboratories, Murray Hill, NJ, USA. He was the Chief Technology Officer (CTO) of Intpax Inc., San Jose, CA, from 2001 to 2003. He was the CTO of Siargo Inc., Santo Clara, CA, from 2004 to 2010. He was a Professor and the Head of the CJ Huang Information Technology Research Institute with Wuhan University, Wuhan, China, from 2004 to 2013. He was the Chief Scientist with Lorentz Solution Inc., Santa Clara, CA, from 2010 to 2013. He is currently a Distinguished Professor with Hangzhou Dianzi University, Hangzhou, China. He has authored over 160 journal articles and holds 22 patents. His current research interests include integrated circuit and microelectromechanical system design and simulation, computational electromagnetics, electronic design automation, and wavelet applications in engineering.

**Xudong Chen** (Fellow, IEEE) received the B.S. and M.S. degrees in electrical engineering from Zhejiang University, China, in 1999 and 2001, respectively, and the Ph.D. degree from the Massachusetts Institute of Technology, Cambridge, MA, USA, in 2005. Since 2005, he has been with the National University of Singapore, Singapore, where he is currently a Professor. He has published 150 journal articles on inverse scattering problems, material parameter retrieval, microscopy, and optical encryption. He has authored the book *Computational Methods for Electromagnetic Inverse Scattering* (Wiley-IEEE, 2018). His research interests include mainly electromagnetic wave theories and applications, with a focus on inverse problems and computational imaging. He is working on mm-wave imaging algorithms and solving inverse problems via machine learning. He is a Fellow of Electromagnetics Academy. He was a recipient of the Young Scientist Award by the Union Radio Scientifique Internationale in 2010, and the Ulrich L. Rohde Innovative Conference Paper Award at ICCEM 2019. He was an Associate Editor of the IEEE TRANSACTIONS ON MICROWAVE THEORY AND TECHNIQUES from 2015 to 2019.